The *HST* Key Project on the Extragalactic Distance Scale XIII. The Metallicity Dependence of the Cepheid Distance Scale [1] [2]

Robert C. Kennicutt, Jr.,[3] Peter B. Stetson,[4] Abhijit Saha,[5] Dan Kelson,[6] Daya M. Rawson,[7] Shoko Sakai,[8] Barry F. Madore,[8] Jeremy R. Mould,[7] Wendy L. Freedman,[9] Fabio Bresolin,[3] Laura Ferrarese,[10] Holland Ford,[11] Brad K. Gibson,[7] John A. Graham,[12] Mingsheng Han,[13] Paul Harding,[3] John G. Hoessel,[13] John P. Huchra,[14] Shaun M.G. Hughes,[15] Garth D. Illingworth,[6] Lucas M. Macri,[14] Randy L. Phelps,[9] Nancy A. Silbermann,[8] Anne M. Turner,[3] and Peter R. Wood[7]

[1]Based on observations with the NASA/ESA *Hubble Space Telescope* obtained at the Space Telescope Science Institute, which is operated by AURA, Inc. under NASA Contract No. NAS5-26555.

[2]Observations reported here have been obtained in part with the Muliple Mirror Telescope (MMT), a joint facility of the University of Arizona and the Smithsonian Institution.

[3]Steward Observatory, University of Arizona, Tucson, AZ 85721

[4]Dominion Astrophysical Observatory, Victoria, British Columbia V8X 4M6 Canada

[5]Space Telescope Science Institute, 3700 San Martin Drive, Baltimore, MD 21218

[6]Lick Observatory, University of California, Santa Cruz, CA 95064

[7]Mount Stromlo and Siding Spring Observatories, Institute of Advanced Studies, ANU, ACT 2611 Australia

[8]Infrared Processing and Analysis Center, California Institute of Technology, Pasadena, CA 91125

[9]Observatories of the Carnegie Institution of Washington, Pasadena CA 91101

[10]Department of Astronomy, California Institute of Technology, Pasadena, CA 91125

[11]Department of Physics and Astronomy, Johns Hopkins University, Baltimore, MD 21218

[12]Department of Terrestrial Magnetism, Carnegie Institution of Washington, Washington D.C. 20015

[13]Department of Astronomy, University of Wisconsin, 475 North Charter Street, Madison, Wisconsin 53706

[14]Harvard Smithsonian Center for Astrophysics, 60 Garden Street, Cambridge, MA 02138

[15]Royal Greenwich Observatory, Cambridge CB3 0EZ England, UK

ABSTRACT

Uncertainty in the metal abundance dependence of the Cepheid variable period-luminosity (PL) relation remains one of the outstanding sources of systematic error in the extragalactic distance scale and the Hubble constant. To test for such a metallicity dependence, we have used the Wide Field Planetary Camera 2 (WFPC2) on the *Hubble Space Telescope* (*HST*) to observe Cepheids in two fields in the nearby spiral galaxy M101, which span a range in oxygen abundance of 0.7 ± 0.15 dex. A differential analysis of the PL relations in V and I in the two fields yields a marginally significant change in the inferred distance modulus on metal abundance, with $\delta(m-M)_0/\delta[O/H] = -0.24 \pm 0.16$ mag dex^{-1}. The trend is in the theoretically predicted sense that metal-rich Cepheids appear brighter and closer than metal-poor stars. External comparisions of Cepheid distances with those derived from three other distance indicators, in particular the tip of the red giant branch method, further constrain the magnitude of any Z-dependence of the PL relation at V and I. The overall effects of any metallicity dependence on the distance scale derived with *HST* will be of the order of a few percent or less for most applications, though distances to individual galaxies at the extremes of the metal abundance range may be affected at the 10% level.

Subject headings: Cepheids — galaxies: distances and redshifts — galaxies: individual (M101, NGC 5457) — cosmology: distance scale

1. Introduction

Cepheid variable stars play a central role in the calibration of the extragalactic distance scale and the Hubble constant (H_0). The measurement of Cepheid distances to a dozen galaxies with the *HST* has led to dramatic improvements in the calibration of the several secondary distance indicators, and narrowed the longstanding discrepancy between the "long" and "short" distance scales from $40-100$ km s^{-1} Mpc^{-1} a few years ago to $\sim 55-75$ km s^{-1} Mpc^{-1} currently (e.g., Saha et al. 1997; Madore et al. 1997). The completion of the *HST* Key Project on the Extragalactic Distance Scale will double again the number of galaxies with Cepheid distances, furnish firm calibrations of the Tully-Fisher (T-F), surface brightness fluctuation (SBF), planetary nebula (PNLF) and globular cluster luminosity functions, SN II expanding parallax, and SN Ia secondary distance indicators, and determine H_0 to an accuracy of $\pm 10\%$ (Kennicutt, Freedman, & Mould 1995).

As the uncertainty in the distance scale as a whole is reduced, systematic uncertainties in the Cepheid distances themselves become increasingly important, because errors in the Cepheid scale propagate with nearly full weight into the secondary distance ladder and H_0. Of particular concern is whether the Cepheid period-luminosity (PL) relation varies systematically with metal abundance. The metal abundances in the Key Project galaxy sample vary by nearly an order of magnitude (Zaritsky, Kennicutt, & Huchra 1994; hereafter ZKH). Current calibrations of the PL relation are referenced to the Large Magellanic Cloud, which has a lower metal abundance ([O/H] $\simeq -0.4$) than is often found in more luminous galaxies in the Key Project sample. Thus a significant Z-dependence to the PL relation could introduce a systematic error in the overall distance scale, as well as an increased scatter in individual distances.

Several theoretical and observational studies argue for a significant metallicity dependence, though the magnitude of the effect remains controversial. Theoretical models by Chiosi, Wood, & Capitanio (1993; hereafter CWC93) predict a small change in the PL zeropoint at visual and near-infrared wavelengths, of order 0.1 mag per factor of ten increase in abundance, but earlier calculations predicted a stronger effect (e.g., Stothers 1988), and the theoretical models remain uncertain (§2).

Evidence for larger effects have come from several recent empirical studies. Freedman & Madore (1990) undertook the first direct observational test of the metallicity dependence of the PL relation, using $BVRI$ photometry of Cepheids in three fields in M31. They derived a change in distance modulus of -0.32 ± 0.21 mag dex^{-1}, a difference which they did not regard as significant. Their data were subsequently reanalyzed by Gould (1994), who derived steeper dependences of -0.88 ± 0.16 and -0.56 ± 0.20 mag dex^{-1}, depending on the bandpasses used in the fitting. Recently Beaulieu et al. (1997) and Sasselov et al. (1997) analyzed EROS data for large samples of Cepheids in the LMC and SMC, and derived a change in inferred distance modulus of $-0.44^{+0.1}_{-0.2}$ mag dex^{-1}. Kochanek (1997) derived a similar dependence of -0.4 ± 0.2 mag dex^{-1} , using published Cepheid measurements of 17 galaxies. Most of the dependence arises from increased line blanketing and redder intrinsic colors at higher abundance, an effect that has been reported in Galactic and Magellanic Cloud Cepheids by several authors (e.g., Caldwell & Coulson 1986; Laney & Stobie 1994, and references therein).

All of these results are consistent with a metallicity dependence that tends to cause the distances of metal-rich Cepheids to be underestimated. However the magnitudes of these claimed dependences range over an order of magnitude, so the significance of any Z-dependence for the distance scale remains unclear. A zeropoint change at the level of $\leq$0.3 mag dex^{-1} would have minimal effects on the ultimate distance scale, because the

Cepheid target galaxies observed with *HST* bracket a large metallicity range with a mean value close to that of the LMC Cepheids that calibrate the PL relation (§6). However dependences as large as those derived by Gould (1994) would introduce systematic errors in H_0 at the 10–20% level, and constitute the dominant systematic error in the entire extragalactic distance ladder. As pointed out by Sasselov et al (1997) and Kochanek (1997), a strong metallicity dependence might account for part of the difference between low values of H_0 determined from SN Ia and other secondary indicators, if the Cepheid abundances in the SN Ia hosts are systematically lower. Such effects might also partly explain the longstanding difference in Cepheid and RR Lyrae distance scales in nearby galaxies. It is imperative to test whether systematic errors at this level are present in the Cepheid data.

As part of the *HST* Key Project we undertook a further test of the metallicity dependence of the PL relation, by targeting two fields in the giant Sc I spiral M101 (Kennicutt et al. 1995). M101 is especially well suited for a metallicity test, because it combines an unusually steep radial abundance gradient with a large disk scale length, making it possible to identify Cepheids with *HST* nearly to the center of the galaxy. The fields we targeted differ in metal abundance by a factor of five, and bracket the abundance range between the LMC and the most metal-rich Cepheid fields observed with *HST*. In this paper we present a *differential* analysis of the Cepheid PL relations in the two fields. Our approach differs from that taken in most of the previous studies, insofar as we direct our attention solely to the effects of abundance on the V and I PL relations used in most of the *HST* Cepheid observations. We apply the same PL fitting methods and abundance calibrations that are applied to other Key Project observations, so that we can place direct limits on the effects of abundance variations on the *HST* Cepheid distance scale, independent of any possible Cepheid metallicity dependence at other wavelengths. We have also compared Cepheid distances to 23 galaxies, spanning a 50-fold range in abundance, with distances derived from three other methods, the tip of the red giant branch method (TRGB), the planetary nebula luminosity function (PNLF), and the Tully-Fisher (TF) method, to further constrain the magnitude of any metallicity dependence.

The paper is organized as follows. In §2 we briefly summarize the effects of abundance on Cepheid magnitudes and colors as expected from theory, and present a series of simulations that quantify the effects on the V and I PL fits used in the *HST* observations. §3 describes the differential test in M101 and the derived metallicity dependence. We compare the results to previous work in §4. In §5 we use TRGB, PNLF, and TF distances to further constrain the metallicity dependence. Finally, in §6 we assess the impact of the dependence on the overall distance scale, and discuss the prospects for a definitive calibration of the Z dependence.

2. Theoretical Expectations and Simulations

The effects of metal abundance on the Cepheid instability strip have been investigated by Stothers (1988), Stift (1990; 1995), and CWC93. The main predictions are that metal-rich Cepheids at a given period are more luminous and redder. The net effects on the observed PL relations are strongly wavelength dependent; metal-rich Cepheids will appear fainter in the blue due to line blanketing, while in the red the sense of the effect is to make the Cepheids appear brighter. The magnitudes of the metallicity effects are also strongly wavelength dependent. In this paper we are concerned solely with the behavior of the PL relations in V and I, which is most relevant to *HST* observations.

The methodology used to fit the PL relations observed in the Key Project is described in Freedman et al. (1994) and Ferrarese et al. (1996). Briefly, the Cepheid target fields are observed at 12 epochs in V (F555W), and at $4-8$ epochs in I (F814W). The observed PL relations at V and I are fitted with slopes fixed to those of the calibrating PL relations in the LMC (Madore & Freedman 1991):

$$M_V = -2.76 \log P - 1.40 \tag{1}$$

$$M_I = -3.06 \log P - 1.81 \tag{2}$$

These calibrations assume an LMC true distance modulus of 18.50 ± 0.10 and an average reddening $E(B-V) = 0.10$, corresponding to $E(V-I) = 0.13$. Any difference in the apparent V and I moduli is assumed to be caused by reddening, and the true modulus is computed assuming $A_V/A_I = 1.666$, or $A_V/E(V-I) = 2.50$ (Cardelli, Clayton, & Mathis 1989). This is the same value found by Stanek (1996).

There are several ways in which metallicity effects could propagate into the Cepheid distances derived in this way. Aside from directly influencing the absolute magnitudes of the Cepheids, any systematic change in $V-I$ color will propagate through the reddening correction and alter the inferred true modulus. CWC93 used analytical fits to their theoretical models to predict the magnitude of these effects for PL relations observed in BV and VI. For a mean period of 10 days, their models predict $\delta(m-M)_0 = +22.2\delta Z$ from fitting PL relations in B and V, but only $-1.7\delta Z$ when fitted in V and I, where Z is the metal mass fraction ($Z_\odot = 0.02$). The VI dependence corresponds to a systematic error of only 0.06 mag in true modulus (3% in distance) between $0.2-2\ Z_\odot$, approximately the full range found in the Cepheid galaxies observed with *HST*. Such a weak dependence would be virtually impossible to measure in the *HST* data. The predicted effects on distances derived from photometry in B and V would be much larger, 44% (or 0.8 mag) for the same abundance range.

However there are other, more subtle ways in which abundance effects might propagate, for example in the way that the width of the Cepheid instability strip and the colors of the blue and red edges are affected (CWC93). In order to incorporate these effects, we constructed simulated Cepheid data sets for different metal abundances and foreground reddenings, and analyzed them using the standard Key Project reduction procedures. Simulated PL relations for a given metallicity Z were derived using the equations given in CWC93. Cepheid masses were then randomly drawn from a mass distribution given by $dn/dm = m^{-3}$ over the mass range $3 - 13\ M_{\odot}$. Luminosities were calculated from equation (25) of CWC93, and the red and blue edges of the instability strip were derived using equations (7) and (13) of the same paper. Stars were randomly positioned between the red and blue edges of the strip, and periods were then calculated from the P–M–L–T$_{eff}$ relation given in equation (4) of CWC93. We used fits to the (BC_V,T_{eff}) and ($V - I$, T_{eff}) relations to derive the apparent V and I magnitudes. Reddening was then added assuming $E(V - I) = 1.31E(B - V)$ and $A(V) = 3.1E(B - V)$.[16] Nine samples of 100 Cepheids each were constructed, with metal abundances $Z = 0.01$, 0.02, and 0.03, and reddening $E(B-V) = 0.1$ and 0.2 mag. The simulated data sets were then fitted to PL relations in V and I, following the standard procedures described earlier. The results are summarized in Table 1. The first three columns of the table are the input values to the simulation, while the last four columns are derived quantities.

We then determined the coefficient in equation (3) by minimizing the difference between $(m - M)_{true}$ and $(m - M)_{PL}$.

$$(m - M)_{true} = (m - M)_{PL} + (0.11 \pm 0.03)\ \log(Z/Z_{LMC}) \tag{3}$$

Throughout this paper we will use the notation γ to denote the change in inferred true distance modulus per factor of ten in metal abundance (cf. Beaulieu et al. 1997; Kochanek 1997), with a subscript indicating the relevant wavelengths over which the PL relation is fitted (V and I unless indicated otherwise). Thus for our simulations $\gamma_{VI} = -0.11 \pm 0.03$ mag dex^{-1}.

The metallicity effect derived in our simulations is slightly larger than the analytical approximation of CWC93, but is still very slight, amounting to a distance error of less than 6% for an order of magnitude change in metal abundance. The sign of the change is in the sense that the distance inferred at higher metal abundances is smaller (Cepheids appear brighter). Unfortunately the theoretical prediction is not robust. For example, the

[16]These reddening coefficients differ slightly from those used in our standard data reductions, but the difference is not significant for this application.

theoretical prediction of the position of the red edge of the instability strip is poorly defined by theory, because of large uncertainties in the theory of convective transport. More recent calculations by Chiosi, Wood, & Capitanio (1997), using new opacities, predict $\gamma_{VI} = +0.06$ mag dex^{-1}, a smaller effect but one in the opposite sense. Although it is reassuring that the metallicity dependence predicted by theory is small, we cannot yet use theory as the basis of a correction to observed distance moduli. Moreover it would be very useful to have independent observational confirmation of the magnitude of the metallicity effects, if not an empirical calibration of the dependence.

3. A Differential Test in M101

The magnitude of the Z-dependence of the PL relation can be measured directly, by observing Cepheids with different metal abundances in the same galaxy. This approach was introduced by Freedman & Madore (1990), who applied the method to M31 using groundbased $BVRI$ CCD photometry. As part of the *HST* Key Project, we observed Cepheids in two fields in the giant Sc galaxy M101. The "inner" and "outer" fields are centered at $14^{\rm h}03^{\rm m}23^{\rm s}.94$, $+54°21'35''.7$ and $14^{\rm h}02^{\rm m}22^{\rm s}.49$, $+54°17'58''.3$ (2000.0), at galactocentric radii of $1'.7$ and $7'.9$, respectively. Figure 1 shows a groundbased image of M101 with the inner and outer WFPC2 field locations superimposed.

3.1. Abundances

The disk abundances in M101 are among the best studied of any galaxy, thanks to several HII region surveys (Kennicutt & Garnett 1996 and references therein). The HII region abundances are measured in terms of oxygen, and we will parametrize the Cepheid metallicity dependence in terms of the nebular oxygen scale using the usual notation: [O/H] $\equiv \log(O/H)/(O/H)_\odot$, and adopting $(O/H)_\odot = 7.9 \times 10^{-4}$. We adopt this convention because metal abundances for most of the Key Project Cepheid fields have been measured from HII region spectra (ZKH). The abundances of the Cepheids themselves could differ slightly from those of the HII regions, either because the stellar iron and oxygen abundances do not scale precisely, or from a small calibration offset between the stellar and interstellar abundances. Neither of these effects is likely to be important, however, because the long-period Cepheids observed with *HST* ($P > 10$ days) arise from relatively massive ($M > 7\ M_\odot$) and shortlived ($< 10^8$ yr) progenitors (CWC93), and variations in [O/Fe] are likely to be small in this young population (Wheeler, Sneden, & Truran 1989). There may be a larger absolute shift between the nebular and stellar abundance scales, but this is

unimportant for the present application, as long as we calibrate and apply the abundance test in a self-consistent manner across the Key Project sample.

Figure 2 shows the HII region abundance distribution over the relevant range of radii in M101, with the locations of the Cepheid fields indicated by the horizontal lines. The solid points are "empirical" abundances based on the strengths of the reddening-corrected [OII]λ3727, [OIII]λ4959,5007, and Hβ lines, taken from the survey of Kennicutt & Garnett (1996), and calibrated following ZKH. The inner Cepheid field contains three HII regions measured in this survey, as indicated by the open circles. The outer Cepheid field contains two bright HII regions that were not included in the Kennicutt & Garnett (1996) survey. Spectra for these objects have been obtained subsequently using the Blue Channel Spectrograph on the Multiple Mirror Telescope, and their abundances are also shown with open circles in Fig. 2. The errors in the empirical abundances (shown in Fig. 2) are dominated by systematic uncertainty in the calibration of the absolute abundance scale, especially at high metallicities, where the calibration rests entirely on theoretical photoionization models. Fitting to the empirical abundance distribution yields a difference between the inner and outer Cepheid fields of $+0.66 \pm 0.20$ dex.

More robust abundances based on measured forbidden-line electron temperatures are available for a handful of HII regions in M101, and these data are shown as open triangles in Fig. 2. The innermost point comes from Kinkel & Rosa (1994), with the other data coming from Kennicutt & Garnett (in preparation). These data show a significant offset from the empirical abundances over part of the radial range, but the difference between the inner and outer fields is very similar, $+0.71 \pm 0.17$ dex, depending on whether the outermost points (NGC 5471) are included. We adopt the average difference of $+0.68 \pm 0.15$ dex. Thus the inner and outer Cepheid fields span nearly a factor of five in abundance.

3.2. *HST* Photometry

Observations of the M101 Cepheid fields were carried out in Cycles 3–5 for the outer field and Cycles 4–5 for the inner field. Details of the respective data sets, including complete discussions of the Cepheid photometry, variable identification, and period determinations can be found in separate papers by Kelson et al. (1996) and Stetson et al. (1997) for the outer and inner fields, respectively.

Several technical obstacles prohibit a direct comparison of the inner and outer field photometry in their entirety. The bulk of the observations of the outer M101 field were obtained before the *HST* refurbishment mission with the original Wide Field Camera

(WFC), whereas the inner field was observed entirely in Cycles 4–5 with WFPC2. Uncertainties in cross-calibrating WFC and WFPC2 could easily mask any real difference in the magnitudes and colors of the Cepheids (cf. Kelson et al. 1996). Fortunately we were able to obtain several exposures of the outer field with WFPC2, and these form the basis of the differential photometry analyzed here. To complicate matters further, most of the WFPC2 observations were obtained early in Cycle 4, when the operating temperature of the camera was adjusted to reduce charge transfer efficiency problems (Holtzman et al. 1995). The WFPC2 data set includes a mix of "warm" and "cold" observations, and the zeropoint calibrations of these data may differ. The combined uncertainties in tying together the WFC vs WFPC2 data and the warm vs cold WFPC2 data could easily amount to several hundredths of a magnitude in $V - I$ color, and mask (or mimic) any signature of a metallicity effect.

To avoid these problems we adopted a completely differential approach to the photometry of the inner and outer fields. Our WFPC2 observations include 5 pairs of visits, when exposures of both fields were taken with the same filter, focus, and camera temperature. These epochs (3 in V and 2 in I) were used to define a common photometric scale for both fields. Table 2 lists the journal of observations for this subset of the data. The other (extensive) observations of each field were used to identify the Cepheid variables and measure their light curves, periods, and phases (Kelson et al. 1996; Stetson et al. 1997), but the magnitude scales used in this paper were determined solely from the 5 WFPC2 epochs listed in Table 2.

The primary set of photometry was performed with the DAOPHOT/ALLFRAME package (Stetson 1994). Details of the reduction and calibration procedures can be found in Hill et al. (1997) and Stetson et al. (1997). The inner and outer field data were reduced using identical point spread functions, aperture corrections, and zeropoint calibrations applied to the two data sets, to minimize the potential for any systematic photometric offset. As a check on our results we performed an independent reduction of the photometry using the DoPhot package (Schecter, Mateo, & Saha 1993). To simplify the presentation we will first describe the main ALLFRAME analysis, followed by a summary of the final results from both reductions.

3.3. Cepheid Samples and Period-Luminosity Relations

Cepheid variables were identified independently for the outer and inner fields by Kelson et al. (1996) and Stetson et al. (1997), respectively. Of the 29 Cepheids identified in the outer WFC field, 26 fell within the field of our WFPC2 images and were cleanly

resolved in our ALLFRAME data. The periods of these stars range from $13 - 58$ days. For the inner field we identified a sample of 50 high-quality Cepheids with large amplitudes, well-determined light curves, and periods in the range $10 - 60$ days, and which appear to be free of crowding, as determined by the PSF fits and from visual inspection of the WFPC2 images (Stetson et al. 1997).

The final product of the ALLFRAME run was 5 V and 2 I magnitudes for each star in the outer field, and 4 V and 2 I magnitudes for the inner field (some epochs contained cosmic ray split exposures). These were averaged to produce intensity-weighted mean magnitudes for each Cepheid. The average photometric errors returned by ALLFRAME for the stars in this magnitude range are ± 0.10 mag in V and I, and as low as ± 0.04 for the brighter Cepheids. The largest source of random error in the magnitudes is the variability of the Cepheids themselves. Because the data were taken at a small number of random phases, our average magnitudes will show a considerable scatter about the true mean values. For the inner field data, we were able to reduce this problem by phase matching the observations to the full light curves and determining true mean magnitudes (but on the photometric zeropoint of the epochs in Table 2). This was not done for the outer field Cepheids, because of the long interval between the main WFC observations that define the light curves, and the larger photometric uncertainties in the WFC magnitudes. We confirmed that this procedure does not introduce any systematic shift in the PL zeropoints.

The resulting PL relations for the inner and outer fields are shown in Figures 3 and 4, respectively. Superimposed in each case are the calibrating PL relations for the LMC, shifted to the best fitting distance modulus. Least squares solutions, constrained to the slopes of the LMC PL relations, yield V and I moduli for the inner field of $\mu_V = 29.59 \pm 0.06$ mag and $\mu_I = 29.43 \pm 0.05$ mag. The corresponding solutions for the outer field are $\mu_V = 29.39 \pm 0.07$ mag and $\mu_I = 29.39 \pm 0.06$ mag. Note that these solutions are based solely on the subset of WFPC2 observations listed in Table 2, and are strictly applicable only for the differential comparison of the inner and outer fields presented here. Fully calibrated magnitudes and PL fits for the fields can be found in Kelson et al. (1996) and Stetson et al. (1997).

In the standard fitting procedure used in the Key Project, the difference in V and I moduli is assumed to represent the average reddening of the Cepheids; hence $E(V - I) = 0.16 \pm 0.03$ mag for the inner field and 0.00 ± 0.04 mag for the outer field. Applying the Cardelli et al. (1989) reddening curve yields for the true moduli $\mu_0 = 29.20 \pm 0.07$ mag for the inner field and $\mu_0 = 29.39 \pm 0.08$ mag for the outer field. These errors include only the uncertainty introduced by the dispersion of the PL relations (the errors in true modulus are comparable to those in V and I individually because the

residuals in the two bandpasses are correlated). The errors in the absolute distance to M101 would be larger, because of additional uncertainties in the photometric zeropoints, the LMC distance and reddening, and other systematics, but these cancel out in the differential comparison. Table 3 summarizes the results of these fits. The results quoted here refer to the complete Cepheid samples in each field, combined for the four WFPC2 detectors. The fits for the complete Cepheid samples yield a difference in inferred true distance modulus of -0.19 ± 0.10 mag, in the theoretically predicted sense (metal-rich closer).

A possible source of concern in this comparison is the difference in the Cepheid period distributions between the two fields. Most of the Cepheids in the outer field have periods longer than 16 days ($\log P \geq 1.2$), whereas the inner field Cepheids are more heavily weighted to the period range $\log P = 1.0 - 1.4$. The absence of short-period variables in the outer field is entirely an observational artifact, caused by interruptions in the observing sequence combined with the brighter magnitude limit in the WFC data. This difference in periods could introduce a spurious difference in distance moduli between the two fields, if the slopes of the PL relations differ significantly from the canonical LMC values used in the fitting. To minimize any bias from this effect we refitted the PL relations, restricting the data to Cepheids with $\log P \geq 1.2$; this includes 24 of the 26 Cepheids in the outer field and 30 of the 50 Cepheids in the inner field. In addition, we excluded 2 Cepheids in the inner field with very red colors ($V - I > 1.5$). Fits to these long-period subsamples yield true moduli for the inner and outer fields of 29.21 ± 0.09 mag and 29.34 ± 0.08 mag, respectively, or an inner $-$ outer difference of -0.13 ± 0.11 mag (Table 3). The average distance modulus we derive for the outer field, 29.36 ± 0.08 mag, is in excellent agreement with the value 29.34 ± 0.17 mag (including all error terms) derived from the original photometry of the M101 Cepheids by Kelson et al. (1996). The outer field abundance is nearly the same as the LMC, which calibrates the PL relation, so its distance modulus is the appropriate one to apply to M101.

The same analysis was performed using the DoPhot photometry package (Schechter, Mateo, & Saha 1993). A list of Cepheid candidates was generated independently, and cross-checked with the final ALLFRAME list, yielding 34 Cepheids in the inner field and 24 in the outer field. The PL relations were then fitted following the same procedures. Fitting the complete Cepheid sets ($P = 10 - 60$ days) yielded a inner $-$ outer difference in true distance modulus of -0.18 ± 0.11 mag (*vs* -0.19 ± 0.10 mag for ALLFRAME). A comparison using only Cepheids with $P = 16 - 60$ days yields a difference of -0.15 ± 0.12 mag (*vs* -0.13 ± 0.11 mag for ALLFRAME). The two analyses yield nearly identical values for the metallicity effect in M101. At first glance it might appear that the agreement is *too* good, given the relatively large uncertainties, but recall that the same stars are being measured, and the quoted uncertainties largely reflect other factors, such as the

intrinsic dispersion of the PL relation, which affect both data sets uniformly. However the consistency of the DoPhot vs ALLFRAME comparison does offer some assurance that the apparent difference in PL relations between the inner and outer fields is not an artifact of field crowding errors in the data reduction.

We adopt for our final result the average of these fits, for a net difference of -0.165 ± 0.10 mag. Combining this with the observed difference in oxygen abundance of $+0.68 \pm 0.15$ dex (§3.1) gives a metallicity dependence:

$$\gamma_{VI} = -0.24 \pm 0.16 \text{ mag dex}^{-1}. \quad (4)$$

The quoted uncertainty includes errors in the Cepheid photometry and in the abundance gradient. Note that the measured Z-dependence is only significant at the 1.5 σ level.

3.4. Interpretation

Theoretical models predict that the Cepheid metallicity dependence is produced by a combination of brighter mean magnitudes and redder colors with increasing metallicity (e.g., CWC93). Observational evidence for systematic changes in the magnitudes and/or colors of Cepheids with abundance has been offered by several authors, including Caldwell & Coulson (1986), Gieren et al. (1993), Laney & Stobie (1994), Sasselov et al. (1997), and Kochanek (1997). With our V and I photometry alone, it is impossible to separate the effects of changes in intrinsic luminosity, intrinsic color, and reddening. However we can use the M101 results along those from other Cepheid data sets to place useful limits on these contributions.

The nature of the shift in the PL relation between the M101 inner and outer fields is illustrated in Figure 5, which shows the residuals of individual Cepheids from the best fitting ALLFRAME V and I PL relations in each field. The top and middle panels show the residuals for Cepheids in the outer and inner fields, respectively, relative to the respective PL fits in those fields. The solid line in each case shows the expected trajectory due to variations in temperature (position in the instability strip), while the dashed line shows the (nearly degenerate) trend expected from reddening variations. The behavior of the residuals in M101 is similar to that seen in all of the Key Project data sets, insofar as most of the dispersion in the PL relations can be attributed to the finite strip width and to reddening variations. The remaining scatter about these correlations are presumably due to a combination of photometric errors and uncertainties in deriving the mean magnitudes from a small number of epochs.

The bottom panel of Figure 5 shows the V and I residuals for stars in the inner field, but in this case with respect to the mean PL relations in the *outer* field. The outer field Cepheids have nearly the same abundances as the LMC Cepheids that calibrate the PL relation, so any metallicity dependence in the PL relation will appear as a systematic residual in this diagram. The inner field Cepheids actually show two distinct differences. First there is a general shift of the distribution to fainter magnitudes in both V and I, along the reddening/temperature trajectory. This we tentatively attribute to a higher mean reddening in the inner field. In addition there is a general shift of stars below the reddening line, which implies that the mean colors of the inner field Cepheids are redder (or else brighter) than would be expected from reddening effects alone. This represents the shift of -0.16 mag in true distance modulus, transformed into the residual plane. The clear appearance of this shift in Figure 5 confirms that the difference in derived distance moduli between the inner and outer fields is significant, and is not merely an artifact of scatter in the PL relations.

We cannot distinguish from V and I data alone whether the shift in distance modulus is produced because the metal-rich Cepheids are brighter at both V and I (with no color change), because the metal-rich stars are intrinsically redder, or from some combination of luminosity and color changes. However the M101 data place bounds on the variation in either extreme. The observed difference in true modulus of 0.16 mag could be produced at constant color by a shift in both V and I moduli of -0.16 mag (trivially), or by a shift in intrinsic color of $+0.08$ mag. Since the abundance difference in the two fields is 0.68 ± 0.15 dex, the implied metallicity dependences would be -0.24 ± 0.16 mag dex^{-1} in luminosity (VI), or 0.12 ± 0.08 mag dex^{-1} in $V - I$ color. In all likelihood some combination of these effects is involved. Note that the observed color excess in the inner field, $E(V - I) = 0.16$ mag, is roughly twice as large as any color difference that can be attributed to metallicity effects. This means that part of the color difference between the Cepheids in the inner and outer fields must be due to interstellar reddening.

Another way to constrain the effects of Z-induced color changes on Cepheid distances is to test whether the observed Cepheid colors correlate systematically with metal abundance. Kochanek (1997) found evidence for such a correlation, based on published photometry for Cepheids in 17 galaxies. We show an updated version of this test in Figure 6. Each point shows the average color excess for Cepheids in a given galaxy (or field), plotted as a function of metal abundance. The color excesses are derived from PL fits in V and I (equations [1] and [2]), with the Galactic foreground reddening subtracted (Burstein & Heiles 1984). The error bars signify the dispersion in the reddenings of individual Cepheids. Data are taken from Kochanek (1997), along with data for IC 1613 (Freedman 1988), the two M101 fields from this paper (open circles), and the three fields in M31 (Freedman & Madore 1990),

shown as crosses. We excluded galaxies in the Kochanek sample with color excesses derived at wavelengths other than V and I, and galaxies without measured HII region abundances. This leaves a sample of 19 fields in 16 galaxies.

Figure 6 shows a clear trend between Cepheid color excess and metallicity, confirming Kochanek (1997). The best fitting slope to our data is $\delta E(V-I)/\delta[O/H] = 0.12 \pm 0.08$ mag dex^{-1} (a linear fit in Z yields virtually the same slope over the relevant abundance range). This color gradient is similar to what is inferred above from the M101 inner and outer fields, but the trend in Figure 6 includes any changes in mean interstellar reddening with metallicity. It is interesting that the color trend is restricted to galaxies with abundances higher than that of the LMC ([O/H] = -0.4), where one might expect a higher dust-to-gas ratio and thus a higher reddening. The absence of a color trend at lower abundances suggests that interstellar reddening may well be responsible for much if not most of the observed color trend. Even if all of the trend in Fig. 6 were due to metallicity effects, it would introduce at most a bias in the distance modulus $\gamma_{VI} \simeq -0.25 \pm 0.17$ mag dex^{-1}.

4. Comparison with Other Studies

The first application of the differential metallicity test for Cepheids over a range of galactocentric distances was carried out for M31 by Freedman & Madore (1990; hereafter FM90). FM90 analyzed random-phase $BVRI$ observations for 38 Cepheids in three fields in M31, located at radii of 3, 10, and 20 kpc. No difference in true distance modulus was detected for the 3 and 10 kpc fields, but the derived true modulus for the 20 kpc field was higher by 0.25 ± 0.17 mag, when determined from the V and I data alone. Combining this with an estimated abundance gradient of 0.75 dex over 3–20 kpc yielded a metallicity dependence $\gamma_{BVRI} = -0.32 \pm 0.21$ mag dex^{-1} and $\gamma_{VI} = -0.39 \pm 0.26$ mag dex^{-1}. FM90 did not solve for γ explicitly, and the numbers listed here were derived from the PL solutions and abundance gradients given in their paper, following Gould (1994). In view of the low statistical significance of this result, FM90 interpreted it as a nondetection, and consistent with no measureable Z dependence of the PL zeropoint.

The M31 data were subsequently reanalyzed by Gould (1994), who used the correlations between magnitude residuals in $BVRI$ in an attempt to separate the effects of metallicity and reddening. His best solutions for the same data yielded values $\gamma_{BVRI} = -0.88 \pm 0.16$ mag dex^{-1} and $\gamma_{BVI} = -0.56 \pm 0.20$ mag dex^{-1}, a much larger and statistically significant dependence. These results cannot are not directly comparable to ours, because the wavelength baseline extends to the blue, where the metallicity effects are expected to be larger. However the analysis illustrates the large range of dependences which are consistent

with the M31 data.

Unfortunately both of these analyses were based on an erroneous value for the abundance gradient in M31. FM90 quoted an abundance range of 0.75 dex over the three Cepheid fields (1.7 to 0.3 solar), citing Blair, Kirshner, & Chevalier (1982), but the abundance gradient given in the latter paper corresponds to a range of only 0.44 dex, when placed at the FM90 distance. Adding data from Dennefeld & Kunth (1981) and recalibrating the oxygen abundances on the ZKH scale lowers the abundance range further to 0.31 ± 0.16 dex over the 3 Cepheid fields (from 1.8 to 0.9 solar). Applying this correction to the FM90 PL solutions changes their metallicity dependence to $\gamma_{VI} = -0.94 \pm 0.78$ mag dex^{-1}, with the larger fractional error reflecting the additional uncertainty in the abundance gradient. Likewise the revised Gould (1994) solutions become $\gamma_{BVRI} = -2.1 \pm 1.1$ mag dex^{-1} and $\gamma_{BVI} = -1.4 \pm 0.8$ mag dex^{-1}. We conclude, in agreement with FM90, that the existing M31 data do not offer very stringent constraints on the Cepheid metallicity dependence. Ongoing efforts to obtain more precise photometry over a wider wavelength baseline may improve the constraints (Kaluzny et al. 1997; Freedman et al. 1997).

A different approach to constraining the metallicity dependence has been employed by Beaulieu et al. (1997), Sasselov et al. (1997) and Kochanek (1997). Beaulieu et al. and Sasselov et al. have compiled a large database of photometry of LMC and SMC Cepheids from the EROS microlensing project, and applied a differential multivariate analysis to determine the maximum likelihood change in distance moduli and color with metallicity. They derive $\gamma_{VI} = -0.44^{+0.1}_{-0.2}$ mag dex^{-1}, This was derived by transforming photometry made at slightly shorter wavelengths (corresponding approximately to Johnson V and R), so the dependence might be slightly steeper than one would derive from V and I photometry.

Kochanek (1997) has applied a similar approach to Cepheid data for 17 galaxies measured from the ground and with *HST*, solving independently for residual extinction and metallicity-dependent colors and luminosities. His maximum likelihood solution yields a mean change in magnitude at V and I of -0.14 ± 0.14 mag dex^{-1} and a $V - I$ color change of 0.13 ± 0.04 mag dex^{-1}. Taken together these would introduce a metallicity dependence in inferred true modulus of $\gamma_{VI} \sim -0.4 \pm 0.2$ mag dex^{-1}. These dependences are larger than the $\gamma_{VI} = -0.24 \pm 0.16$ mag dex^{-1} derived here from our M101 observations, but the results are consistent within their quoted uncertainties.

5. External Tests

The metallicity sensitivity of the Cepheid distance scale can be tested externally if independent distances are available for galaxies spanning a large range in abundance. The tip of the red giant branch (TRGB) method offers a strong test of the Cepheid scale over a large abundance baseline. Two other secondary distance indicators, the planetary nebula luminosity function (PNLF) and the Tully-Fisher (TF) method, provide indirect constraints on the magnitude of the Z effects as well.

5.1. Comparison with TRGB Distances

The TRGB method utilizes the nearly constant luminosity of the red giant branch tip in the I band ($M_I = -4.0 \pm 0.1$). Globular cluster observations by Da Costa & Armandroff (1990) indicate that the tip luminosity remains constant over a large range of metallicity ($-2.2 < [Fe/H] < -0.7$), and theoretical isochrones show a similar constancy over the same abundance range, and for ages of $2 - 15$ Gyr (Lee, Freedman, & Madore 1993; Madore, Freedman, & Sakai 1997, and references therein). The method has been applied to 9 galaxies with independently determined Cepheid distances, as summarized in Table 4. Included are Cepheid and TRGB distances with their associated uncertainties and the metal abundances of the galaxies. We list two sets of Cepheid distances, the published values and those determined from the PL relations at V and I alone, if different. Testing for a Z dependence in the VI Cepheid data alone is much cleaner, as it avoids problems introduced by a wavelength-dependent metallicity dependence, though the distance moduli determined from V and I alone are often less precise. The abundances listed in Table 4 are determined from HII regions (Skillman, Kennicutt, & Hodge 1989; ZKH), and apply to the Cepheids (not the red giants), because we are testing for metallicity effects in the Population I Cepheids. The galaxies span 7 magnitudes in absolute magnitudes and a factor of 50 in (Pop I) metal abundance, thus providing us with a sensitive test for metallicity effects in the Cepheids. The red giant abundances of the galaxies all lie within the calibrated range of the TRGB method, where metallicity effects in the TRGB distances should be small.

We also include an indirect comparison for two spirals in the Leo I group, NGC 3351 and NGC 3368. These galaxies have *HST* Cepheid distances measured from Graham et al. (1997) and Hjorth & Tanvir (1997), respectively, and a TRGB distance determined for an elliptical member of the group, NGC 3379, from Sakai et al. (1997b). In these cases the comparison may be influenced by group depth, so the data should be accorded lower weight. The TRGB distances for these objects are marked in parentheses in Table 4.

The absolute distances measured with the two methods show good agreement, with an rms scatter of ± 0.16 mag (8% in distance). Figure 7 shows the residuals plotted as a function of metal abundance (NGC 3351 and NGC 3368 are indicated with open circles). There is a slight trend with abundance, and a least squares fit yields a best fitting slope $\gamma_{VI} = -0.16 \pm 0.08$ mag dex^{-1}, shown by the solid line in Figure 7. Comparing to the more heterogeneous set of published Cepheid distances (not all at V and I alone) yields a nearly identical fit ($\gamma = -0.14 \pm 0.08$).

One might worry that these trends could be influenced by a metallicity dependence in the TRGB distances (cf. Saleris & Cassissi 1997). This is very unlikely, however, because the red giant abundances in these galaxies are virtually uncorrelated with the metallicites of the Cepheid fields, and changing them does not appreciably influence the slope of the relation in Figure 7. As a check we recalculated the TRGB distances using a steeper Z dependence for the RR Lyrae luminosity scale, $dM_V(RR)/d[Fe/H] = 0.30$ instead of 0.17 as adopted in Table 4. Repeating the comparison in Figure 7 with the new TRGB distances yielded nearly the same result as before, $\gamma_{VI} = -0.12 \pm 0.08$ mag dex^{-1}, and if anything produces a slightly weaker Cepheid Z dependence. Lee et al. (1993) directly compared TRGB and Cepheid distances as a function of giant branch abundance, and found no significant dependence on (Pop II) metallicity.

Although our analysis has focussed on the Z dependence of the PL relation in V and I, seven of the galaxies in Table 4 have Cepheid distances based on $BVRI$ fits, and we can check whether there is evidence for a significant metallicity dependence in those distances. Repeating the comparision yields very similar results, with $\gamma_{BVRI} = -0.13 \pm 0.11$. Given the small sample and the inhomogeneity of the data set, we regard this as a tentative result. However it is interesting that there is no indication in the TRGB comparison for a strong metallicity dependence, even in the blue.

To summarize, the comparison of Cepheid and TRGB distances yields another marginal detection of a Cepheid metallicity dependence, $\gamma_{VI} = -0.16 \pm 0.08$ mag dex^{-1}, which is formally consistent with our M101 results ($\gamma_{VI} = -0.24$), as well as with the theoretically predicted dependence ($\gamma_{VI} = -0.11$). The dashed and dotted lines in Figure 7 show the dependences that are expected for values of γ between -0.24 and -0.88; the strong dependences suggested by previous studies are not confirmed here. These results, together with our M101 analysis, offer the strongest evidence for a weak metallicity dependence to the PL relations in V and I.

5.2. Other Tests

We can perform a similar check for galaxies with Cepheid and PNLF distances. Direct comparisons are available for 7 galaxies, and indirect comparisons via galaxies in the same group or cluster are available for 4 other Cepheid hosts. The data are listed in Table 4, with the indirect comparisons in parentheses. Most of these data were taken directly from comparisons in Soffner et al. (1996) and Feldmeier, Ciardullo, & Jacoby (1997), with the addition here of abundance values appropriate to the Cepheid fields.

Figure 8 shows the Cepheid − PNLF distance modulus residuals as a function of metal abundance. Again there is an excellent correlation between the absolute distances (± 0.19 mag rms), as shown previously by Soffner et al. (1996) and Feldmeier et al. (1997). This comparison is not as clean as the TRGB test, because the galaxies cover a smaller range in metal abundance, and the PNLF method itself may have a metallicity dependence at the ± 0.2 mag level (Ciardullo & Jacoby 1992). Given these large uncertainties, the PNLF distances do not impose tight constraints on the Cepheid metallicity dependence, and if anything Figure 8 is suggestive of a modest Z dependence in the PNLF distances.

As a final check we can use the slope of the local Tully-Fisher (TF) relation to constrain the magnitude of any Cepheid Z dependence. Distances from the TF method are currently available for 15 Cepheid calibrating galaxies. Unfortunately a residual test of the sort applied to the TRGB and PNLF distances cannot be applied here, because the intrinsic dispersion of the TF relation is much larger, and because one of the parameters in the TF method, galaxy luminosity, is itself strongly correlated with disk metallicity (Garnett & Shields 1987; ZKH). As a result any metallicity dependence in the Cepheids will primarily act to change the apparent slope of the TF relation, rather than affect the scatter of the relation (Gould 1994). We can exploit this effect, however, and test whether the slope of a TF relation calibrated from Cepheid distances is significantly shallower than the slope derived from observations of distant spirals, where relative distances are derived independently of the Cepheid scale. The magnitude of the slope change for a given Cepheid Z-dependence can be easily derived. Consider for example the I-band TF relation:

$$M_I = a \log W + M_I(0) \tag{5}$$

If we define the metallicity dependence γ in the usual way,

$$\gamma = \frac{d(m-M)}{d[O/H]} \tag{6}$$

and define β as the slope of the absolute magnitude vs metallicity relation,

$$\beta = \frac{dM_I}{d[O/H]} \tag{7}$$

then the effect of the Cepheid Z dependence will be to alter the TF slope:

$$\frac{\delta a}{a} = -\frac{\gamma}{\beta} \tag{8}$$

We used the I-band TF analysis of Giovanelli et al. (1997) to derive representative values of a and β. These authors compiled observations of 555 spiral galaxies in 24 rich clusters and applied incompleteness corrections to define the slope of the TF relation independent of the Cepheid scale, yielding $a = -7.67 \pm 0.11$ (bivariate fit). Giovanelli et al. also compiled I magnitudes and linewidths for 15 galaxies with Cepheid distances, including 12 with measured HII region abundances. A least squares fit of absolute magnitude vs [O/H] yields a luminosity-metallicity slope $\beta = 4.8 \pm 1.0$. This is similar to $\beta = 4.6$ from ZKH (but using B magnitudes). Applying $a = -7.67$ and $\beta = 4.8$ to equation (8) then allows us to predict the TF slopes for the Cepheid calibrating galaxies, for various values of γ. The predicted changes in slope range from 5% (to $a = -7.3$) for $\gamma = -0.24$ mag dex^{-1} to 18% ($a = -6.3$) for $\gamma = -0.88$ mag dex^{-1}.

Figure 9 shows the TF relation for the 15 Cepheid calibrating galaxies (Giovanelli et al. 1997), with the predicted slopes superimposed. The slope of the Cepheid-derived TF relation is actually *steeper* than the cluster-calibrated relation. A bivariate fit to the 12 galaxies with reliable linewidths (Giovanelli et al. 1997) yields $a = -8.65 \pm 0.66$. Fitting all 15 galaxies yields an even steeper slope. The slopes of the Cepheid-calibrated relations thus are consistent with no Z dependence, though the large uncertainty in the slope, not unexpected for a small sample, again limits the usefulness of this test. Our slope also agrees with that derived by Pierce & Tully (1988) for the Ursa Major cluster ($a_I = -8.72$), but their linewidths and magnitudes were calibrated using slightly different methods, so we cannot compare our slope directly to theirs. Nevertheless the Tully-Fisher data offer further evidence against a large abundance effect in the Cepheids ($\gamma_{VI} < -0.5$). It should be possible to tighten these limits as more *HST* Cepheid distances are accumulated over the course of the Key Project.

6. Discussion

We begin by summarizing the results of the various tests presented in this paper. The direct comparison of PL relations for the inner and outer Cepheid fields in M101

imply a difference in inferred true distance moduli of 0.16 ± 0.10 mag (inner field closer), over an abundance baseline of 0.68 ± 0.15 dex. This implies a metallicity dependence of distance modulus inferred from V and I PL relations of $\gamma_{VI} = -0.24 \pm 0.16$ mag dex^{-1}. An external comparison of Cepheid distances with those obtained using the TRGB method implies an even smaller dependence: $\gamma_{VI} = -0.16 \pm 0.08$ mag dex^{-1}, over a metallicity range of 1.7 dex. Comparisons with two sets of distance estimates, using the PNLF and Tully-Fisher methods, are consistent with no systematic metallicity dependence within large uncertainties, and they limit the magnitude of any dependence to $\gamma_{VI} \gg -0.5$ mag dex^{-1}. A comparable upper limit is implied by the systematic dependence of Cepheid color on metal abundance. All of these results are consistent with a maximum range in $\gamma_{VI} \simeq -0.25 \pm 0.25$ mag dex^{-1}, when measured from PL relations in V and I. This range is consistent with the very weak sensitivity predicted by theory ($\gamma_{VI} \simeq -0.1$ mag dex^{-1}), or with no dependence at all.

It is important to emphasize that the results quoted here apply only to PL relations measured in the V and I bands. There is theoretical and observational justification for suspecting that the metallicity dependence at bluer wavelengths is considerably stronger, but this is not relevant to the current *HST* measurements, which are carried out exclusively at V and I. Until the magnitude of the Z dependence at bluer wavelengths is well calibrated, it would be prudent to restrict extragalactic applications of Cepheids to observations at V and longer wavelengths.

What are the implications for the distance scale and H_0 of a metallicity dependence in this range? The abundance effects clearly are most important for galaxies with unusually high or low abundances relative to the LMC, which serves as the zeropoint calibrator for the PL relation. On the ZKH calibration the LMC has an oxygen abundance $12 + \log(\mathrm{O/H}) = 8.50$, or $[\mathrm{O/H}] = -0.40$. The most metal-rich galaxies in the Key Project sample reach $[\mathrm{O/H}] \simeq 0.3$ (e.g., NGC 3351, M100, M101 inner field). For $\gamma = -0.24$ mag dex^{-1} the corresponding error in distance is -9% (-0.18 mag), in the sense that distances to the metal-rich galaxies are systematically underestimated. For $\gamma = -0.5$ mag dex^{-1} the distance change is as much as -18%, but this is a hard upper limit, applied to the most metal-rich galaxies observed with *HST*, and computed for the maximum allowable metallicity dependence. It is worth noting that any strong Cepheid metallicity dependence would tend to cause the Cepheid distance to the LMC to be *overestimated*, and compensate partly for the distance effects on more distant metal-rich galaxies.

The Cepheid Z dependence tends to cause the distances of metal-poor galaxies to be overestimated. The abundances of the most metal-poor galaxies in the Key Project are only slightly below that of the LMC (e.g., NGC 3319, with $[\mathrm{O/H}] \sim -0.5$). For those galaxies

the predicted metallicity effects are less than 3%, even for the largest reasonable values of γ. The effects may be larger for some of the SN Ia calibrators being observed by Sandage and collaborators with *HST* (e.g., Saha et al. 1994). Beaulieu et al. (1997) and Kochanek (1997) have suggested that the value of H_0 derived from the SN Ia method may increase by $16 - 24\%$, for an assumed $\gamma_{VI} \simeq -0.4$ mag dex^{-1}. Our analysis suggests a much smaller difference, based on the weaker metallicity dependence observed in M101, and the likelihood that the abundances of the SN Ia calibrators are closer to the LMC than has been assumed by the other authors. The most metal-poor SN Ia calibrator is probably NGC 5253, with [O/H] $\simeq -0.7$ (Webster & Smith 1983), and its distance would have been overestimated by only $0 - 8\%$, for the range of γ considered here.

Given the probable magnitude of these effects, should one apply metallicity corrections to Cepheid distances measured with *HST*? As illustrated above, the effects on individual distances are probably 10% *at most*, and for most galaxies the changes are at the few percent level. Cepheid distances currently measured with *HST* are subject to several random and systematic uncertainties at the 5% level, including uncertainty in the LMC distance, the absolute calibration of the V and I magnitudes measured with WFPC2, and uncertainties in the reddening corrections applied to the WFPC2 photometry (cf. Ferrarese et al. 1996; Hill et al. 1997; Madore et al. 1997). In view of these other errors and the uncertain magnitude of the metal abundance correction itself, we believe that it is most prudent at this time not to apply a metallicity correction to individual Cepheid distances, but rather to include this source of uncertainty in the systematic error budget for the distance. At the end of the Key Project we hope to have better estimates of these uncertainties, and a much improved zeropoint calibration of the PL relation (Kennicutt et al. 1995).

In the meantime, one can assess the importance of metal abundance effects on the overall distance scale. Beaulieu et al. (1997), Sasselov et al. (1997) and Kochanek (1997) explored the consequences of a $\gamma = -0.44$ mag dex^{-1} dependence on currently published measurements of H_0, and concluded that the Key Project H_0 value could be reduced by up to 10%, based on the Virgo cluster calibration of Freedman et al. (1994b) and Mould et al. (1995). However the most recent Key Project H_0 determination is based on a much larger sample of Cepheid distances and secondary distance indicators, and is much less susceptible to this metallicity bias (Madore et al. 1997). As an illustration, Figure 10 shows a histogram of oxygen abundances for the Key Project galaxies with HII region measurements. These include the *HST* target galaxies, with abundances from ZKH, and the groundbased calibrators M31, M33, NGC 300, NGC 2366, NGC 2403, and NGC 3109. Although there is a spread of over an order of magnitude in these abundances, the median value is [O/H] $\simeq -0.3$, nearly identical to the LMC abundance of [O/H] $= -0.4$. Thus the effect of even a substantial Cepheid metallicity dependence will be negligible for any

distance indicator that is calibrated using most or all of the Key Project Cepheid sample (e.g., the Tully-Fisher relation). The net abundance effect will differ for each secondary distance method, depending on the subset of Cepheid calibrating galaxies, but for most methods the mean Cepheid abundance will be solar or below, so the Z effects should be at the 0.10 mag level or less (less than 5% in distance and H_0). The situation is less certain for the SN Ia distance scale, because abundances for most of the Cepheid calibrators have not yet been measured. We are obtaining HII region spectra for the galaxies in order to assess the importance of abundance effects on the SN Ia distance scale.

Systematic metal abundance effects may be more important for galaxies in the Virgo and Fornax clusters. It is well established that spirals in the core of the Virgo cluster are systematically more metal-rich than their field counterparts (Skillman et al. 1996), and this region contains several Cepheid calibrating galaxies (M100, NGC 4548, NGC 4535, NGC 4639, NGC 4571). Less is known about the abundances in the Fornax cluster, but the Key Project sample includes three Fornax members (NGC 1365, NGC 1425, NGC 1326A), and the one spiral with measured abundances (NGC 1365) is relatively metal-rich. It will be important when calibrating H_0 via galaxies in Virgo and Fornax to consider the possible systematic abundance effects. However from the comparisons given earlier the maximum magnitude of an abundance effect will be to underestimate the distances by $\sim$10%, and consequently lead to a decrease in H_0 of 10%.

Our V and I photometry of the two M101 fields provides tentative evidence for a small metallicity dependence of the PL relation at these wavelengths, and when combined with other tests, places firm upper limits on the magnitude of the metallicity effect. These are sufficient to ensure that the overall consequences of a metallicity dependence on the ultimate H_0 calibrations with *HST* are small (at the level of a several percent or less), and comparable to a multitude of other known error sources in the distance scale calibration. However the tests presented in this paper fall far short of establishing a definitive calibration of the PL metallicity dependence. Such a calibration would significantly improve the accuracy of individual Cepheid distance determinations to individual galaxies, and provide valuable constraints on the theoretical understanding of the Cepheids themselves. Here we briefly describe several observations that would address this need. We also refer to reader to Kochanek (1997) for a discussion of this subject.

As has been discussed previously by Madore & Freedman (1985) and Kochanek (1997), the primary limitation of the *HST* observations is the $V - I$ wavelength baseline. This restriction was imposed primarily by the need to maximize observing efficiency on *HST*, and by the absence, until recently, of a near-infrared imaging capability on *HST*. A targeted program aimed at obtaining high precision Cepheid photometry of a single galaxy such as

M101 over a wide wavelength baseline and over a wide range of abundances would enable one to break the degeneracy between reddening and metallicity effects, and accurately calibrate the Z dependence. Groundbased observations of this kind are being obtained by at least two groups for M31. The installation of NICMOS on *HST* makes such a program very feasible in a more distant galaxy with a steeper abundance gradient, such as M101.

The effects of metallicity and reddening on the PL relation are smaller at near-infrared wavelengths (e.g., McGonegal et al. 1982; CWC93), which argues strongly for supplementing the existing WFPC2 V and I photometry of Cepheid calibrating galaxies with NICMOS imaging in H and/or J. As the absolute uncertainty in H_0 approaches the 10% level, the systematic uncertainties associated with metallicity and reddening corrections to the Cepheid distances will become the dominant source of error in the entire extragalactic distance ladder. Thus a modest effort to assess and correct these systematic errors will have great leverage in improving the calibration of individual extragalactic distances, and ultimately the Hubble constant as well.

We are pleased to thank George Jacoby, Chris Kochanek, and Dimitar Sasselov for useful comments and discussions. We also thank the referee for suggesting several improvements to the paper. The work presented in this paper is based on observations made by the NASA/ESA Hubble Space Telescope, obtained by the Space Telescope Science Institute, which is operated by AURA, Inc. under NASA contract No. 5-26555. We gratefully acknowledge the support of the NASA and STScI support staff, with special thanks to Peggy Stanley and Doug Van Orsow. Support for this work was provided by NASA through grant GO-2227-87A from STScI. This research has made use of the NASA/IPAC Extragalactic Database (NED) which is operated by the Jet Propulsion Laboratory, California Institute of Technology, under a contract with the National Aeronautics and Space Administration.

REFERENCES

Beaulieu, J.P. 1997, A&A, 318, L47

Blair, W.P., Kirshner, R.P., & Chevalier, R.A. 1981, ApJ, 247, 879

Burstein, D., & Heiles, C. 1984, ApJS, 54, 33

Caldwell, J.A.R., & Coulson, I.M. 1986, MNRAS, 218, 233

Capaccioli, M., Piotto, G., & Bresolin, F. 1992, AJ, 103, 1151

Cardelli, J.A., Clayton, G.C. & Mathis, J.S. 1989, ApJ, 345, 245

Ciardullo, R., & Jacoby, G.H. 1992, ApJ, 388, 268

Chiosi, C., Wood, P.R., & Capitanio, N. 1993, ApJS, 86, 541 (CWC93)

Chiosi, C., Wood, P.R., & Capitanio, N. 1997, in preparation (CWC97)

Da Costa, G.S., & Armandroff, T.E. 1990, AJ, 100, 162

Dennefeld, M., & Kunth, D. 1981, AJ, 86, 989

Feldmeier, J.J., Ciardullo, R., & Jacoby, G.H. 1997, ApJ, 479, 231

Ferrarese, L. et al. 1996, ApJ, 464, 568

Freedman, W.L. 1988, ApJ, 326, 691

Freedman, W.L., & Madore, B.F. 1990, ApJ, 365, 186 (FM90)

Freedman, W.L., Wilson, C.D., & Madore, B.F. 1991, ApJ, 372, 455

Freedman, W.L. et al. 1992, ApJ, 396, 80

Freedman, W.L. et al. 1994a, ApJ, 427, 628

Freedman, W.L. et al. 1994b, Nature, 371, 757

Freedman, W.L., Madore, B.F., & Sakai, S. 1997, in preparation

Garnett, D.R., & Shields, G.S. 1987, ApJ, 317, 82

Gieren, W.P. 1993, MNRAS, 265, 184

Giovanelli, R., Haynes, M.P., da Costa, L, Freudling, W., Salzer, J., & Wegner, G. 1997, AJ, 113, 53

Graham, J.A. et al. 1997, ApJ, 477, 535

Gould, A. 1994, ApJ, 426, 542

Hill, R. et al. 1997, ApJ, in press

Hjorth, J., & Tanvir, N.R. 1997, ApJ, 482, 68

Holtzman, J. et al. 1995, PASP, 107, 1065

Kaluzny, J., Stanek, K.Z., Krockenberger, Z.Z., Sasselov, D.D., Tonry, J.L., & Mateo, M. 1997, AJ, in press

Kelson, D. et al. 1996, ApJ, 463, 26

Kennicutt, R.C., Freedman, W.L., & Mould, J.R. 1995, AJ, 110,1476

Kennicutt, R.C., & Garnett, D.R. 1996, ApJ, 456, 504

Kennicutt, R.C., & Bresolin, F. 1997, in preparation

Kinkel, U., & Rosa, M.R. 1994, A&A, 282, L37

Kochanek, C.S. 1997, ApJ, in press

Laney, C.D., & Stobie, R.S. 1994, MNRAS, 266, 441

Lee, M.G., Freedman, W.L., & Madore, B.F. 1993, ApJ, 417, 553

Madore, B.F., & Freedman, W.L. 1985, AJ, 90. 1104

Madore, B.F., & Freedman, W.L. 1991, PASP, 103, 933

Madore, B.F., Freedman, W.L., & Sakai, S. 1997, in The Extragalactic Distance Scale, ed. M. Livio, M. Donahue, & N. Panagia (Cambridge: Cambridge Univ. Press), 239

Madore, B.F. et al. 1997, Nature, submitted

McGonegal, R., McLaran, R.A., McAlary, C.W., & Madore, B.F. 1982, ApJ, 257, L33

McMillan, R., Ciardullo, R., & Jacoby, G.H. 1993, ApJ, 416, 62

Mould, J. et al. 1991, ApJ, 383, 467

Oey, M.S., & Kennicutt, R.C. 1993, ApJ, 411, 137

Pierce, M.J., & Tully, R.B. 1988, ApJ, 330, 579

Richer, M.G., & McCall, M.L. 1995, ApJ, 445, 642

Saha, A. et al. 1994, ApJ, 425, 14

Saha, A. et al. 1995, ApJ, 438, 8

Sakai, S., Madore, B.F., & Freedman, W.L. 1996, ApJ, 461, 713

Sakai, S., Madore, B.F., & Freedman, W.L. 1997a, ApJ, 480, 589

Sakai, S., Madore, B.F., Freedman, W.L., Lauer, T., Ajhar, E.A., & Baum, W.A. 1997b, ApJ, 478, 49

Salaris, M., & Cassissi, S. 1997, MNRAS, 289, 406

Sasselov, D. et al. 1997, A&A, 324, 471

Schechter, P.L., Mateo, M., & Saha, A. 1993, PASP, 105, 1342

Silbermann, N.A. et al. 1996, ApJ, 470, 1

Skillman, E.D., Kennicutt, R.C., & Hodge, P.W. 1989, ApJ, 347, 875

Skillman, E.D., Kennicutt, R.C., Shields, G.S., & Zaritsky, D. 1996, ApJ, 462, 147

Soffner, T., Mendez, R.M., Jacoby, G.H., Ciardullo, R., Roth, M.M., & Kudritzki, R.P. 1996, A&A, 306, 95

Stanek, K.Z. 1996, ApJ, 460, L37

Stetson, P.B. 1994, PASP, 106, 250

Stetson, P.B. et al. 1997, in preparation

Stift, M.J. 1990, A&A, 229, 143

Stift, M.J. 1995, A&A, 301, 776

Stothers, R.B. 1988, ApJ, 329, 772

Webster, B.L., & Smith, M.G. 1983, MNRAS, 204, 743

Wheeler, J.C., Sneden, C., & Truran, J.W. 1989, ARA&A, 27, 279

Zaritsky, D., Kennicutt, R., & Huchra, J. 1994, ApJ, 420, 87 (ZKH)

Figure Captions

FIG. 1.— POSS image of M101 from the Digital Sky Survey, with the locations of the two WFPC2 fields indicated. North is up, east is to the left.

FIG. 2.— Radial abundance distribution in M101, as derived from HII region spectra. The round points and circles are empirical abundances based on the calibration of ZKH. Open circles denote HII regions that are located in the inner and outer Cepheid fields. Open triangles denote abundances based on HII regions with measured electron temperatures. The horizontal lines indicate the radial coverage of the Cepheid fields.

FIG. 3.— Observed Cepheid PL relations from ALLFRAME photometry of the M101 outer field in V (top) and I (bottom). The lines show the least squares fits, constrained to the slope of the LMC calibrating relations.

FIG. 4.— Observed Cepheid PL relations in the M101 inner field. Notation the same as in Fig. 3.

FIG. 5.— Distributions of V and I residuals of individual Cepheids from the PL fits shown in Figs. 2 and 3. The top panel shows residuals of the outer field Cepheids from the outer field fit. The middle panel shows the residuals of inner field Cepheids from the inner field fit. The bottom panel shows the residuals of the inner field Cepheids from the outer field PL fits. In each panel the solid line shows the expected residuals from instability strip width effects, while the dashed line shows the expected trend from reddening variations.

FIG. 6.— Correlation of the average color excess of the Cepheids in a given galaxy or field with abundance. In each case the Galactic foreground reddening has been subtracted. The solid line show the bivariate least squares fit to the correlation.

FIG. 7.— Difference between the distance moduli of nearby galaxies determined from Cepheids and by the TRGB method, plotted as a function of the Cepheid abundances. Solid points indicate direct comparisons of galaxies with Cepheid and TRGB distances, while the open circles indicate indirect comparisons using Cepheid and TRGB distances of different galaxies in Leo I group. The solid line shows a bivariate least squares fit to the relation. The dashed and dotted lines show trends expected for a different Cepheid Z dependences.

FIG. 8.— Similar comparison to Fig. 7, but in this case comparing Cepheid distances with those derived from the PNLF method. Solid points indicate direct comparisons in galaxies with Cepheid and PNLF distances, while open circles are indirect comparisons using different galaxies in the same group. The lines show expected trends as in Fig. 6.

FIG. 9.— The I-band Tully-Fisher relation for Cepheid calibrating galaxies, using data from Giovanelli et al. (1997). The open circles indicate galaxies with poorly determined linewidths, and which are not included in the fit. The solid line shows the best fitting relation. The dashed and dotted lines show the relations expected for different Cepheid Z dependences γ, as in Figs. 6 and 7.

FIG. 10.— Distribution of Cepheid abundances in the Key Project sample, as determined from HII region measurements, on the calibration of ZKH. The vertical line indicates the abundance of the LMC, which defines the PL calibrations.

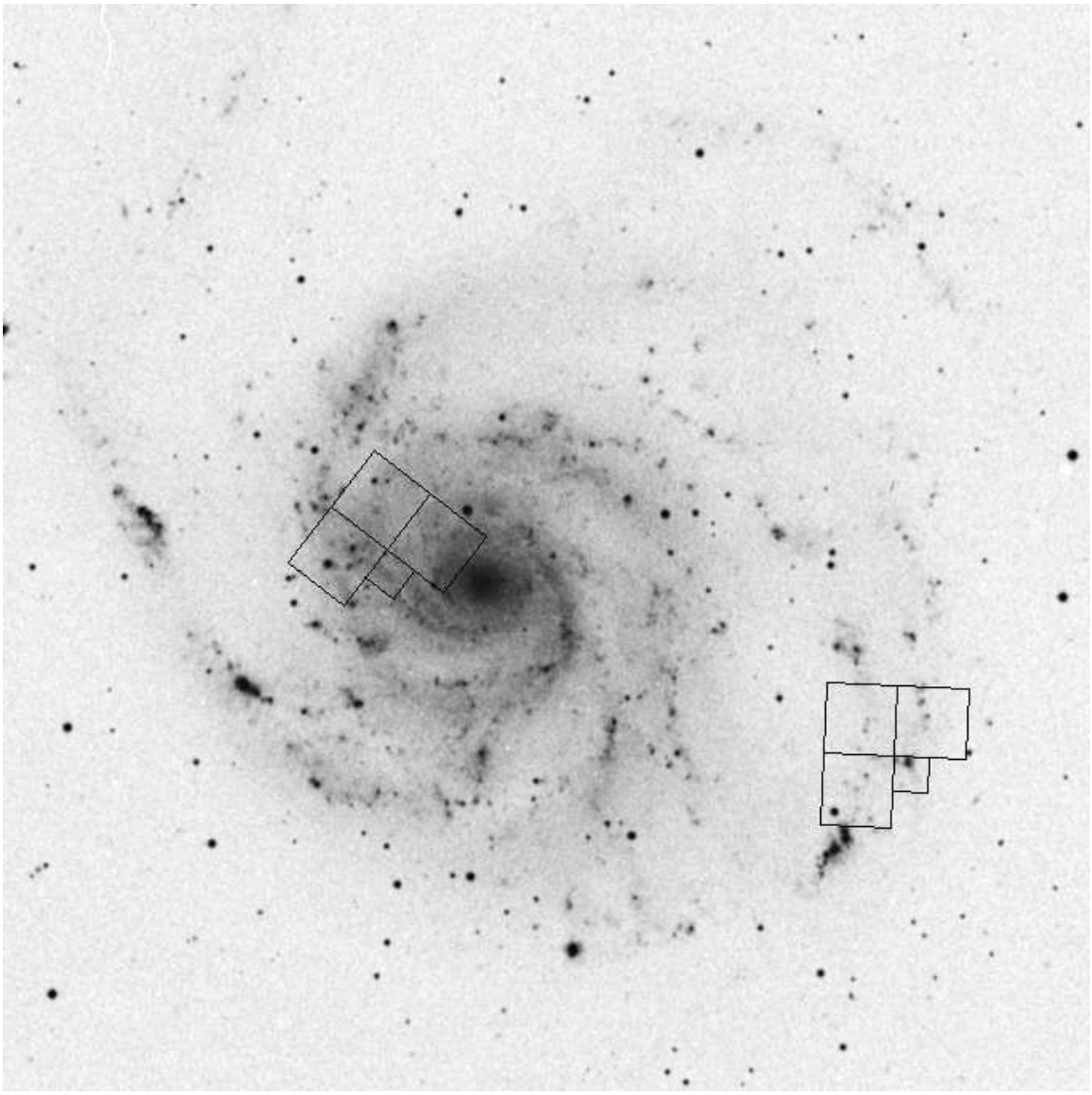

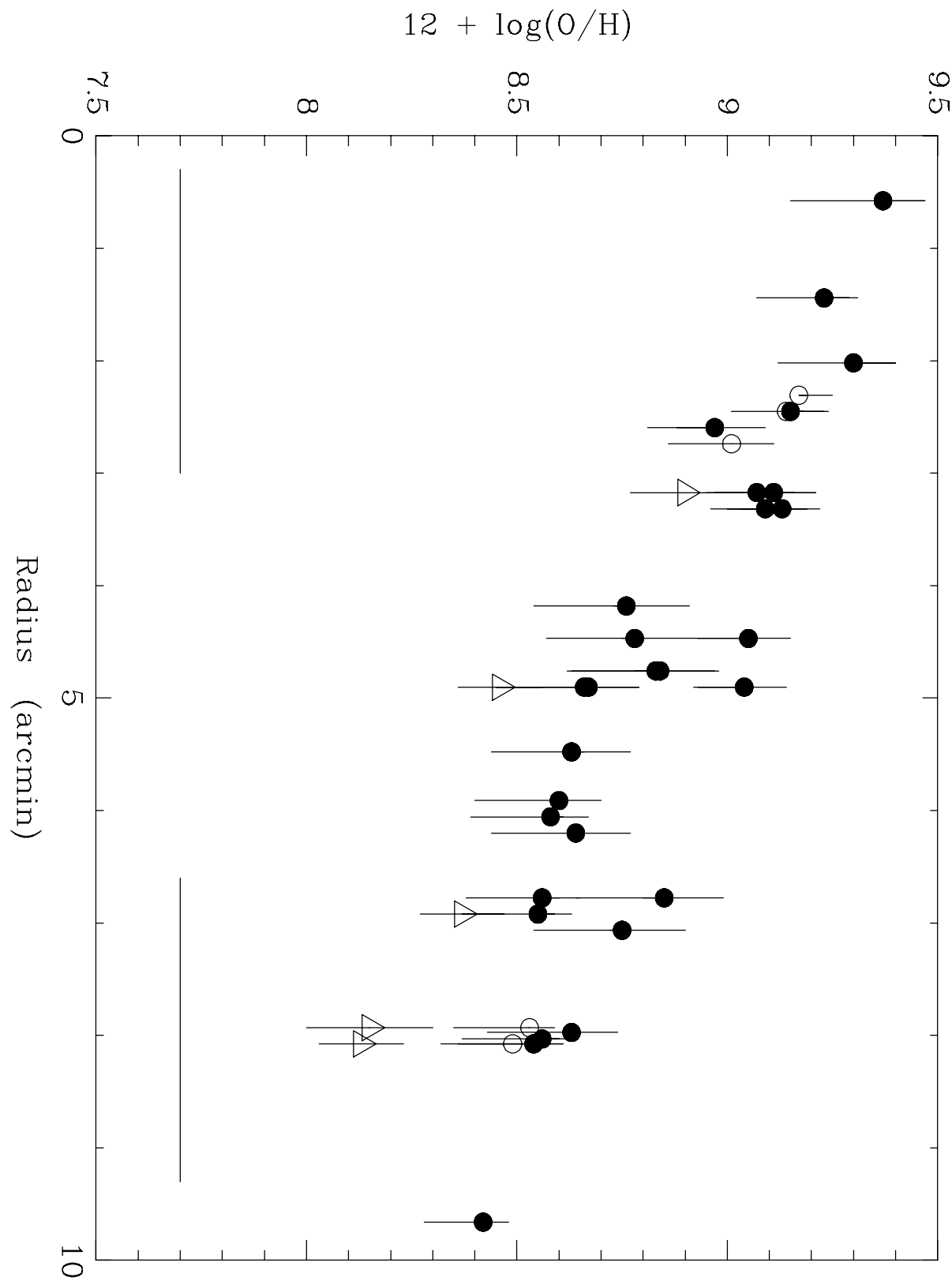
12 + log(O/H)
7.5
8
8.5
9
9.5
0
5
10
Radius (arcmin)

TABLE 2

JOURNAL OF OBSERVATIONS: DIFFERENTIAL TEST

Date	Field	Filter	Exposure Time(s)	Camera Temp	Data Set
1994 Mar 18	Outer	F555W	1200	Warm	U2783103T
1994 Mar 22	Inner	F555W	1200	Warm	U2780101T
1994 Mar 23	Outer	F814W	1200	Warm	U2783201T
1994 Mar 22	Inner	F814W	1000	Warm	U2780102T
1994 Apr 3	Outer	F814W	1200	Warm	U2783301T
1994 Apr 8	Inner	F814W	1200	Warm	U2780302T
1995 Mar 22	Outer	F555W	500 + 500	Cold	U2MS0201T/02T
1995 Mar 22	Inner	F555W	1200	Cold	U2780D01T
1995 Apr 4	Outer	F555W	500 + 500	Cold	U2MS0401T/02T
1995 Apr 17	Inner	F555W	500 + 500	Cold	U2MS0301T/02T

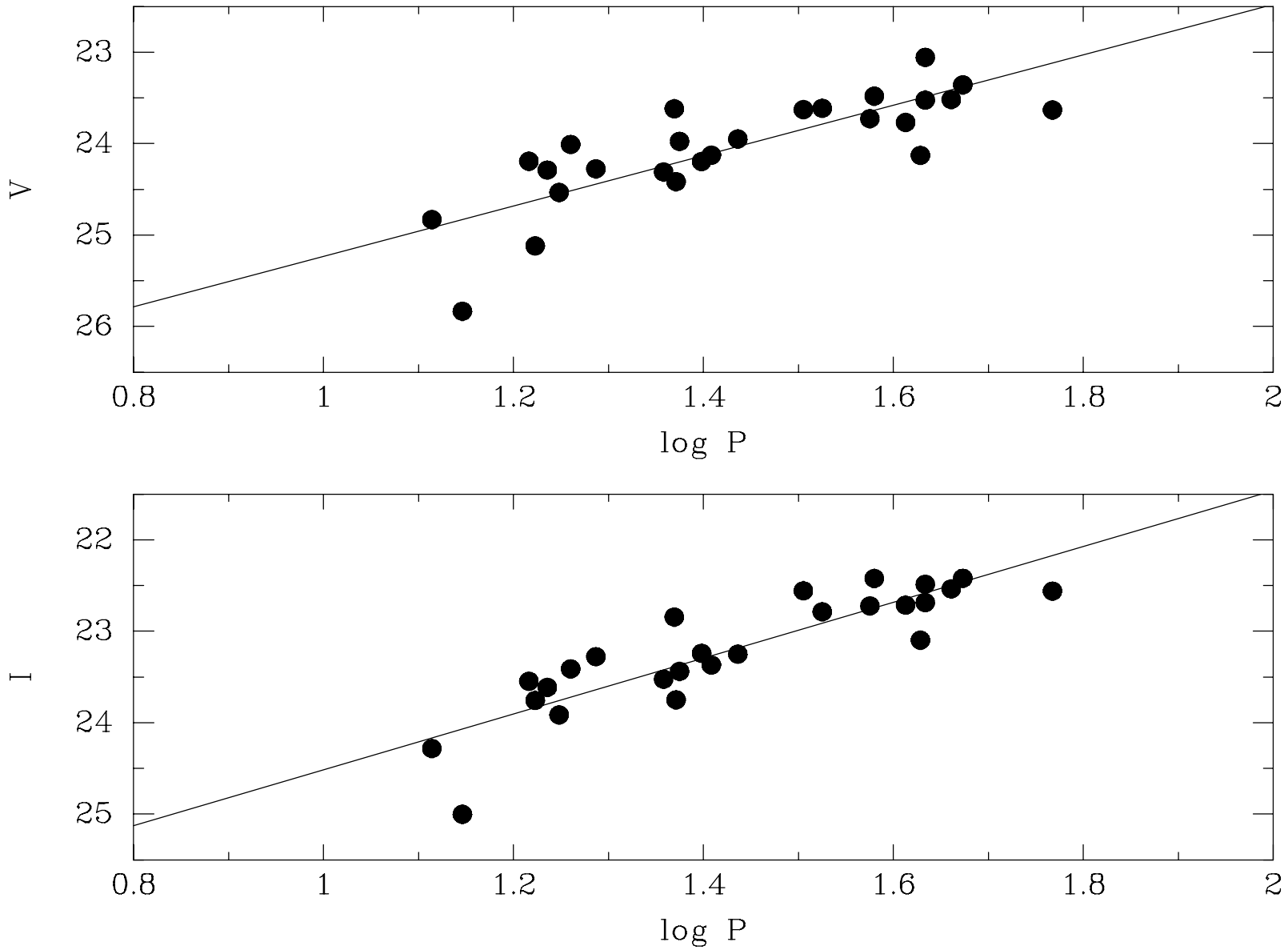

TABLE 3

ALLFRAME Period-Luminosity Relations

Sample	Field	Cepheids	$(m-M)_V$	$(m-M)_I$	$(m-M)_0$	$\delta(m-M)_0$
log P $>$ 1.0	Outer	26	29.39±0.07	29.39±0.06	29.39±0.08	···
	Inner	50	29.59±0.06	29.43±0.05	29.20±0.07	−0.19±0.10
log P $>$ 1.2	Outer	24	29.36±0.06	29.35±0.05	29.34±0.08	···
	Inner	30	29.62±0.08	29.46±0.07	29.21±0.09	−0.13±0.11

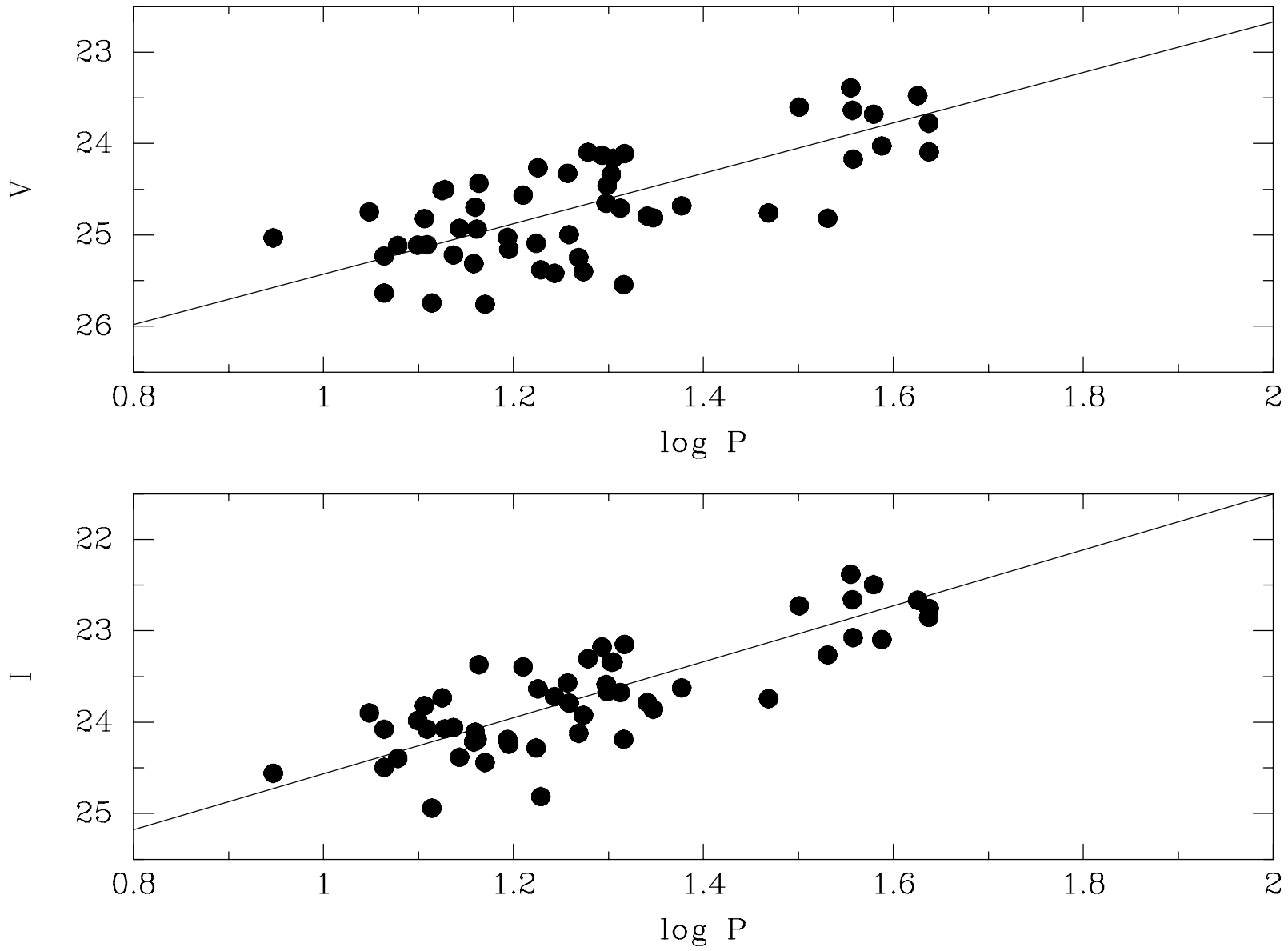

TABLE 4

Comparison of Cepheid, TRGB, and PNLF Distances

Galaxy	$(m-M)_{BVRI}$	$(m-M)_{VI}$	$(m-M)_{TRGB}$	$(m-M)_{PNLF}$	$12+\log(\mathrm{O/H})$	Refs
LMC	18.50±0.10	18.50±0.10	18.42±0.10	$18.49^{+0.12}_{-0.14}$	8.50±0.15	1,2,3
M31	24.42±0.12	24.41±0.12	24.44±0.10	24.44±0.08	8.98±0.15	4,1,2,5
M33	24.63±0.09	24.56±0.10	24.70±0.10	···	8.82±0.15	6,1,5
M81	···	27.80±0.19	···	$27.78^{+0.08}_{-0.09}$	8.75±0.15	7,2,5
M101	···	29.35±0.17	···	$29.43^{+0.09}_{-0.12}$	8.37±0.15	8,2,3
NGC 300	26.70±0.11	26.62±0.15	···	$26.90^{+0.21}_{-0.29}$	8.35±0.15	9,2,5
NGC 925	···	29.84±0.16	···	(29.97±0.12)	8.55±0.15	10,2,5
NGC 1365	···	31.43±0.20	···	(31.14±0.14)	8.96±0.20	11,12,5
NGC 3109	25.67±0.16	25.66±0.20	25.45±0.20	···	8.06±0.15	13,1,14
NGC 3351	···	30.01±0.19	(30.30±0.14)	···	9.24±0.20	15,16,5
NGC 3368	···	30.27±0.13	$(30.30^{+0.08}_{-0.10})$	29.91±0.15	9.20±0.20	17,2,18
NGC 4321	···	31.03±0.17	···	(30.94±0.15)	9.13±0.20	19,2,5
NGC 5253	···	27.93±0.16	···	$27.86^{+0.14}_{-0.46}$	8.15±0.15	20,2,21
NGC 6822	···	23.62±0.20	23.46±0.10	···	8.14±0.15	1,22
IC 1613	24.42±0.13	24.35±0.15	24.27±0.25	···	7.86±0.15	23,1,22
Sextans A	25.85±0.15	25.73±0.17	25.74±0.15	···	7.49±0.15	24,22
Sextans B	25.69±0.27	25.84±0.31	25.56±0.26	···	7.56±0.15	25,22
WLM	···	24.92±0.20	24.81±0.20	···	7.74±0.15	1,22

References.— (1) Lee et al. 1993; (2) Feldmeier et al. 1997; (3) This paper; (4) Freedman & Madore 1990; (5) Zaritsky et al. 1994; (6) Freedman et al. 1991; (7) Freedman et al. 1994a; (8) Kelson et al. 1996; (9) Freedman et al. 1992; (10) Silbermann et al. 1996; (11) Madore et al. 1997; (12) McMillan et al. 1993; (13) Capaccioli et al. 1992; (14) Richer & McCall 1995; (15) Graham et al. 1997; (16) Sakai et al. 1996b; (17) Hjorth & Tanvir (1997); (18) Oey & Kennicutt 1993; (19) Ferrarese et al. 1996; (20) Saha et al. 1995; (21) Webster & Smith 1983; (22) Skillman et al. 1989; (23) Freedman 1988; (24) Sakai et al. 1996; (25) Sakai et al. 1997a.

δV
−1
−0.5
0
0.5
1
1.5
δI
Outer/Inner
Inner
Outer

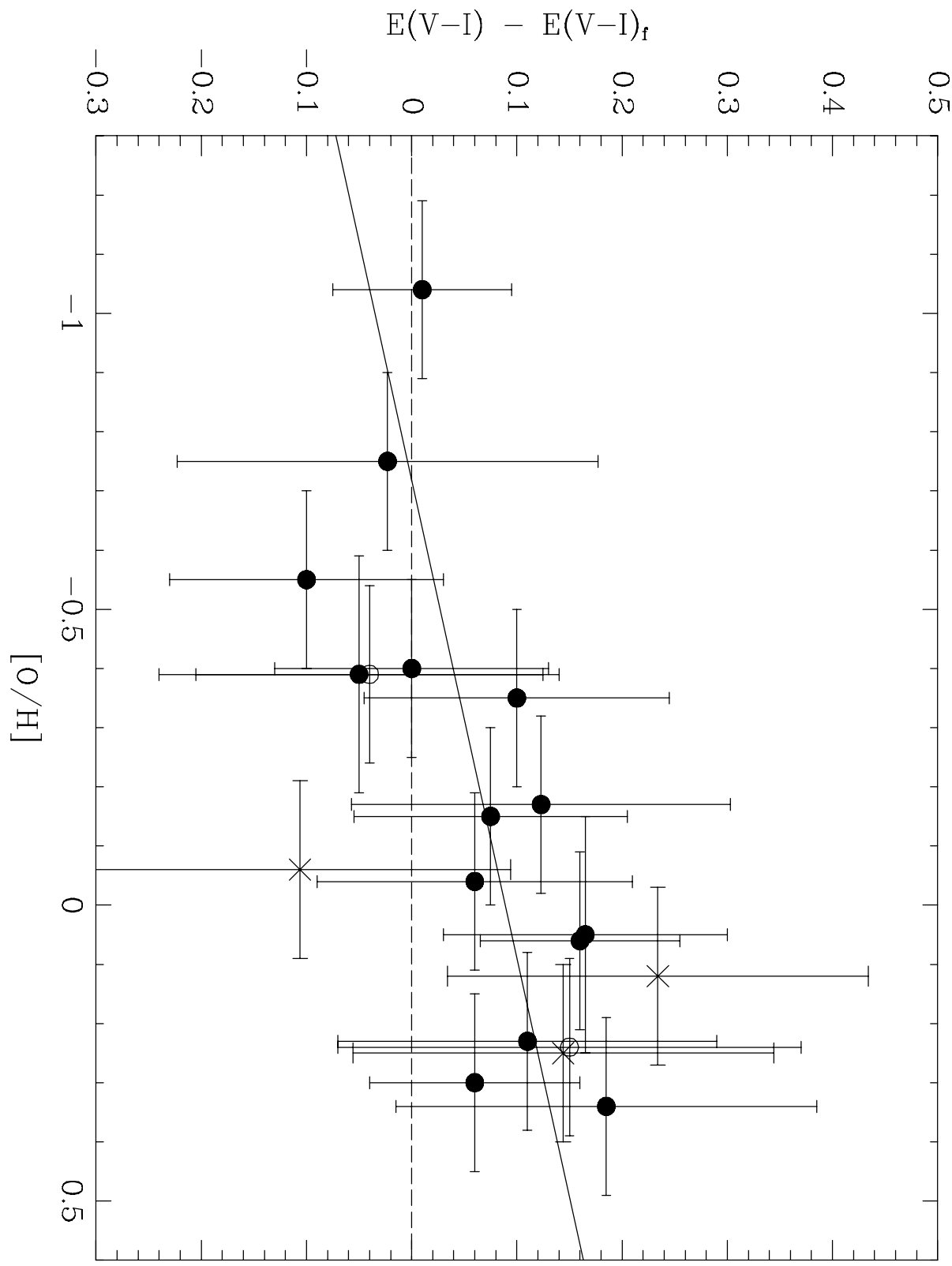
E(V−I) − E(V−I)f
−0.3
−0.2
−0.1
0
0.1
0.2
0.3
0.4
0.5
[H/O]
−1
−0.5
0
0.5

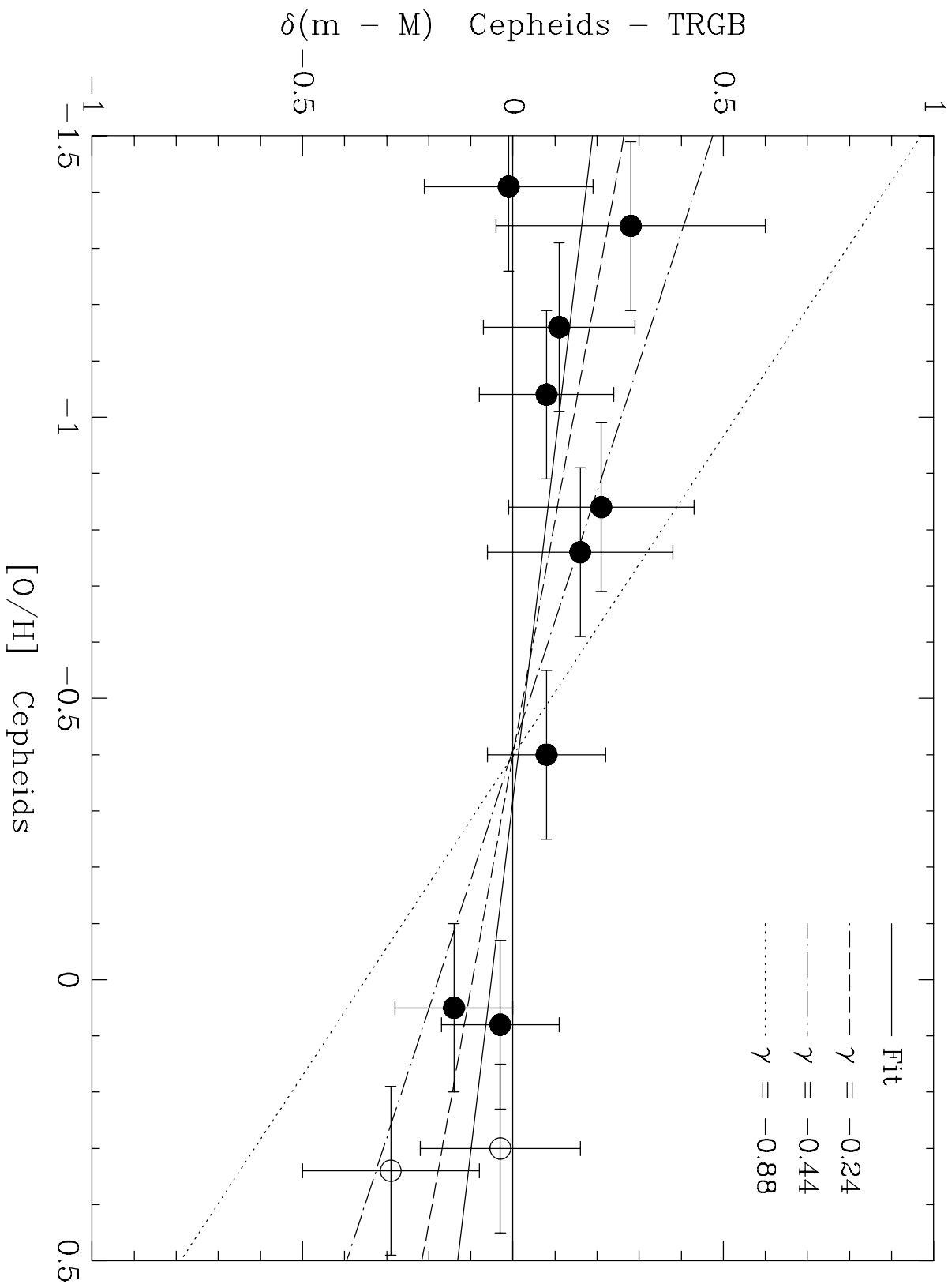
δ(m − M) Cepheids − TRGB
−0.5
0
0.5
1
−1
−1.5
−1
−0.5
0
0.5
[O/H] Cepheids
Fit
γ = −0.24
γ = −0.44
γ = −0.88

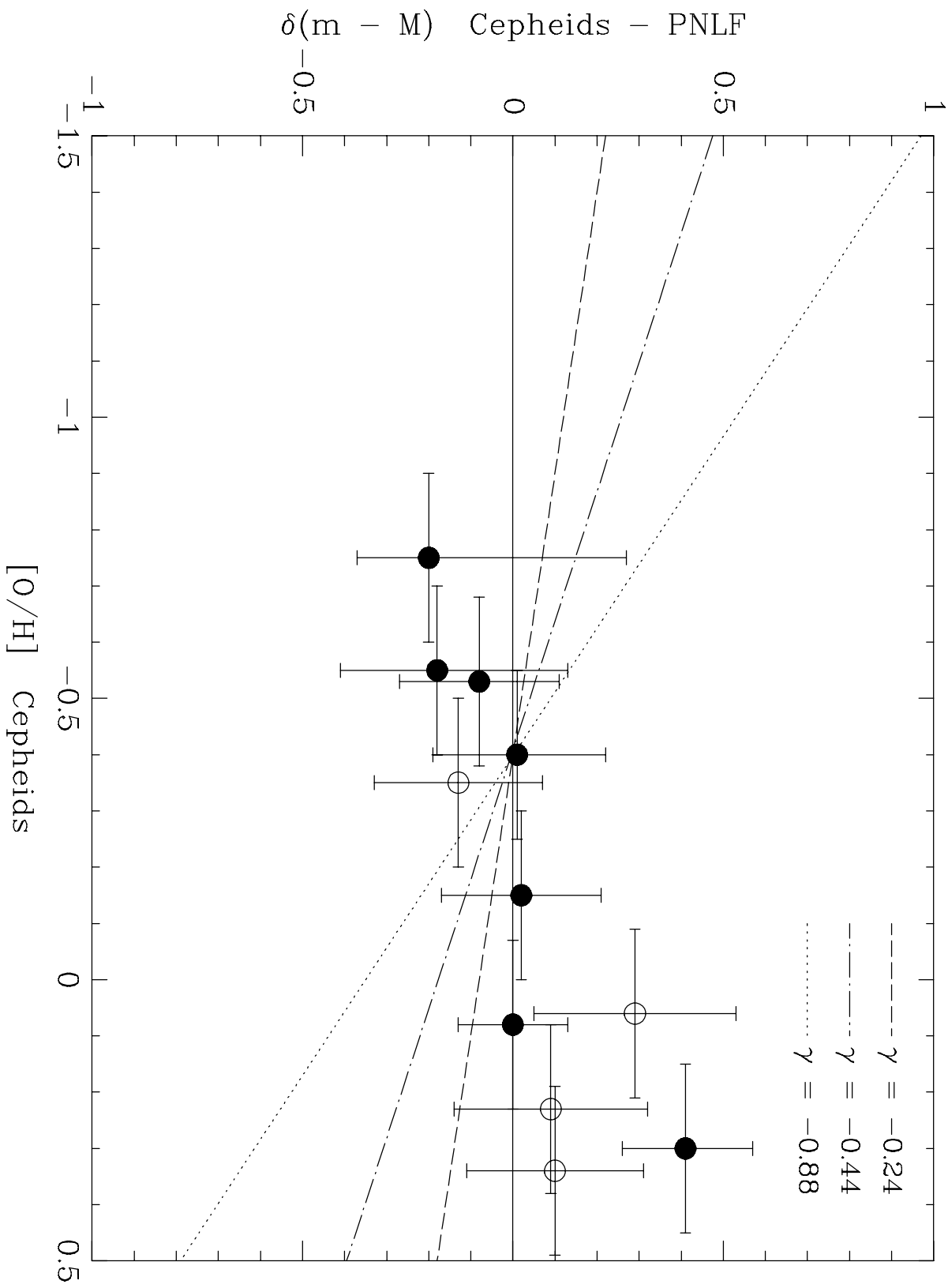
δ(m − M) Cepheids − PNLF
[O/H] Cepheids
−1
−1.5
−0.5
0
0.5
1
γ = −0.24
γ = −0.44
γ = −0.88

log W
1.8
2
2.2
2.4
2.6
2.8
−16
−18
−20
−22
−24
M_I
Fit
$\gamma = -0.25$
$\gamma = -0.88$

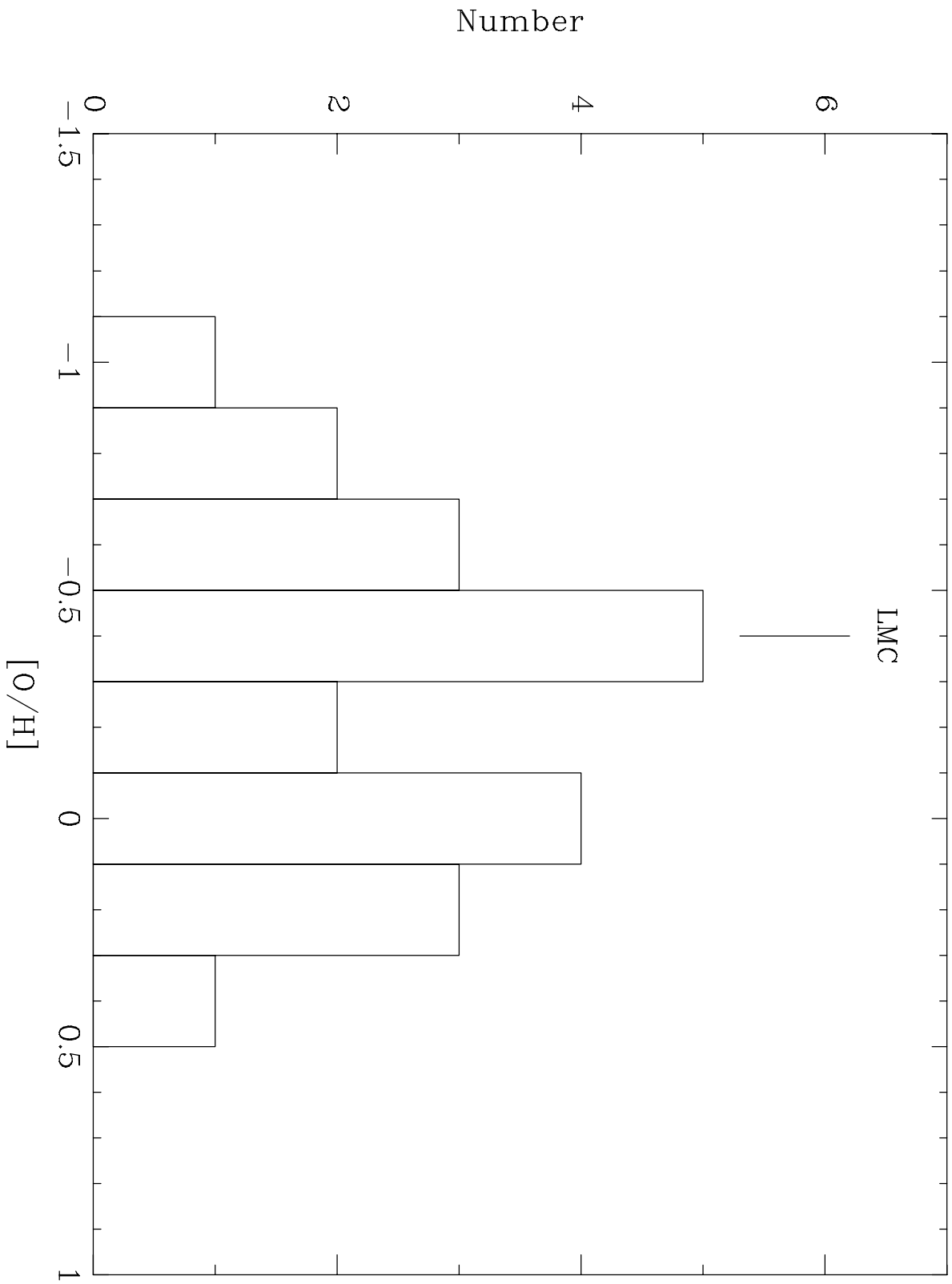
Number
0
2
4
6
−1.5
−1
−0.5
0
0.5
1
[O/H]
LMC

TABLE 1

Period Luminosity Metallicity Simulation Data

#	Z	E(B–V)	m-M	$(m\text{-}M)_V$	$(m\text{-}M)_I$	E(V–I)	$(m\text{-}M)_0$
CWC97							
1	0.01	0.1	31.5	31.77±0.02	31.65±0.02	0.12 ±0.01	31.48±0.01
2	0.02	0.1	31.0	31.33±0.02	31.18±0.02	0.15 ±0.01	30.96±0.01
3	0.03	0.1	31.0	31.46±0.04	31.28±0.03	0.18 ±0.01	31.01±0.01
4	0.02	0.2	31.0	31.64±0.02	31.36±0.02	0.28 ±0.01	30.95±0.02
5	0.03	0.2	31.0	31.72±0.03	31.42±0.03	0.30 ±0.01	30.97±0.02
6	0.01	0.1	31.0	31.25±0.02	31.13±0.01	0.30 ±0.01	30.97±0.02
7	0.03	0.1	31.5	31.97±0.04	31.79±0.03	0.19 ±0.01	31.52±0.02
8	0.01	0.2	31.0	31.56±0.02	31.32±0.02	0.25 ±0.01	30.96±0.01
9	0.02	0.1	31.5	31.85±0.02	31.69±0.02	0.15 ±0.01	31.47±0.01
CWC93							
1	0.02	0.2	31.2	31.83±0.03	31.57±0.02	0.25 ±0.01	31.21±0.01
2	0.03	0.2	31.2	31.88±0.04	31.60±0.02	0.29 ±0.01	31.18±0.01
3	0.01	0.1	31.2	31.46±0.02	31.38±0.02	0.09 ±0.01	31.25±0.01
4	0.03	0.1	31.7	32.03±0.03	31.88±0.02	0.14 ±0.01	31.68±0.01
5	0.01	0.2	31.2	31.74±0.02	31.53±0.02	0.21 ±0.01	31.23±0.01
6	0.02	0.1	31.7	32.05±0.02	31.92±0.02	0.13 ±0.01	31.74±0.01
7	0.03	0.1	31.2	31.60±0.03	31.44±0.02	0.16 ±0.01	31.20±0.01
8	0.02	0.1	31.2	31.58±0.03	31.44±0.02	0.14 ±0.01	31.24±0.01
9	0.01	0.1	31.7	32.02±0.02	31.92±0.02	0.10 ±0.01	31.77±0.01